

Supplementary figures:

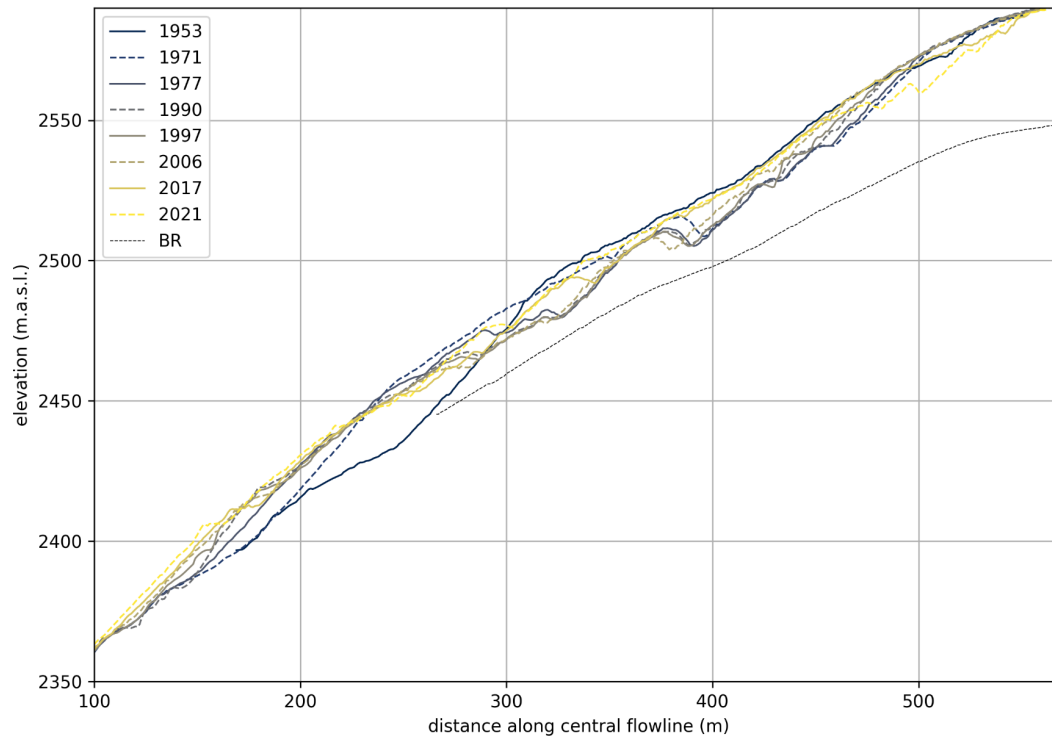


Fig. S1: Surface elevation along the flow line as extracted from the DSMs for selected years, zoomed in on the rock glacier terminus. Estimated bedrock profile (dashed line) from Hartl et al. 2016.

(Hartl, L., Fischer, A., Klug, C. & Nicholson, L. (2016) *Can a simple Numerical Model Help to Fine-Tune the Analysis of Ground-Penetrating Radar Data? Hohebenkar Rock Glacier as a Case Study*, *Arctic, Antarctic, and Alpine Research*, 48:2, 377-393, DOI: 10.1657/AAAR0014-081)

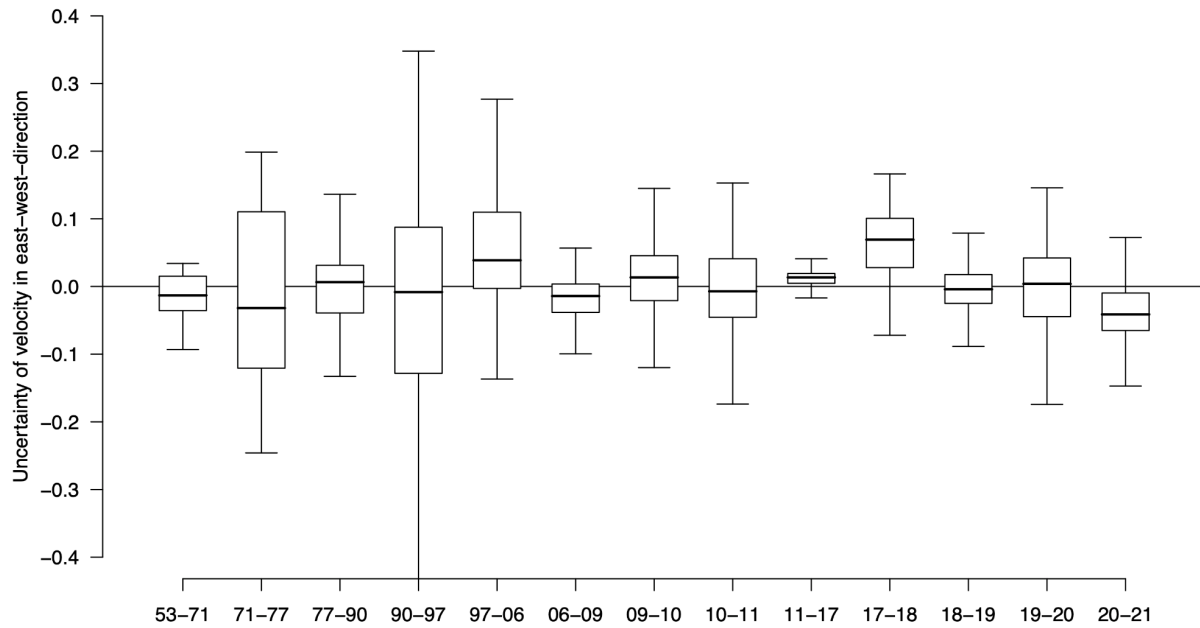


Fig. S2: Uncertainty of velocity in east-west direction for each DSM pair (m/a).

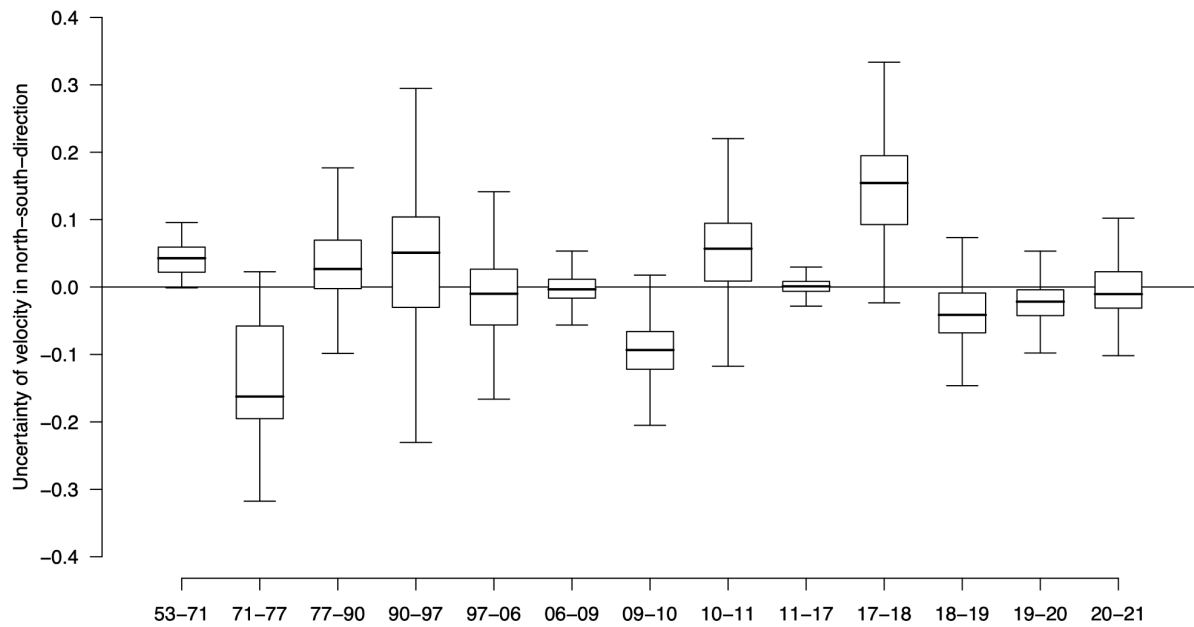


Fig. S3: Uncertainty of velocity in north-south direction for each DSM pair (m/a).

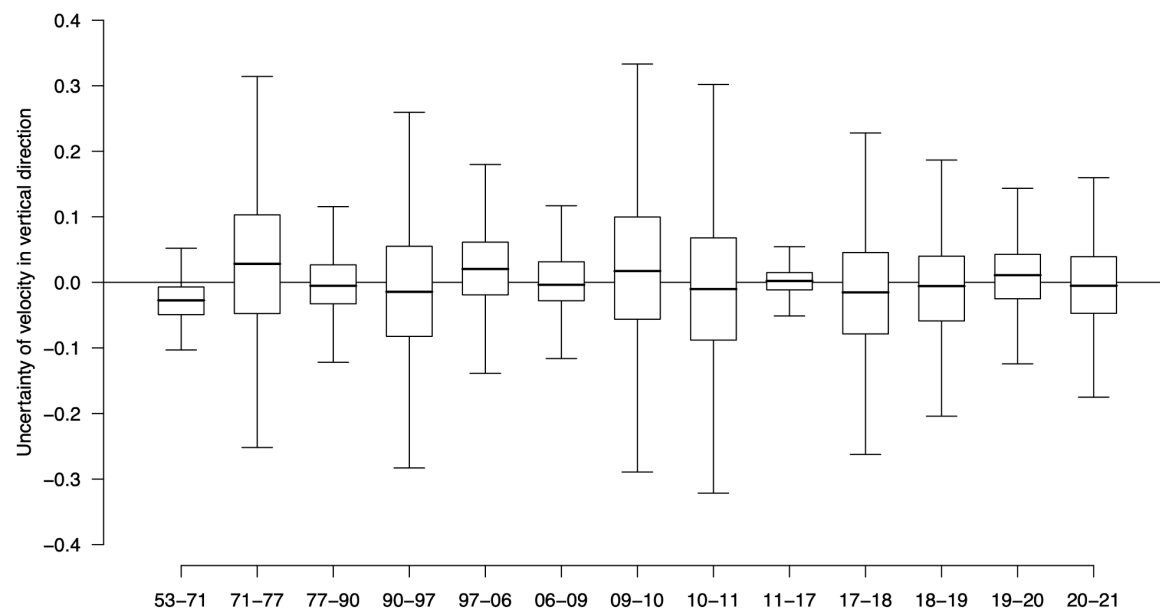


Fig. S4: Uncertainty of velocity in vertical direction for each DSM pair (m/a).

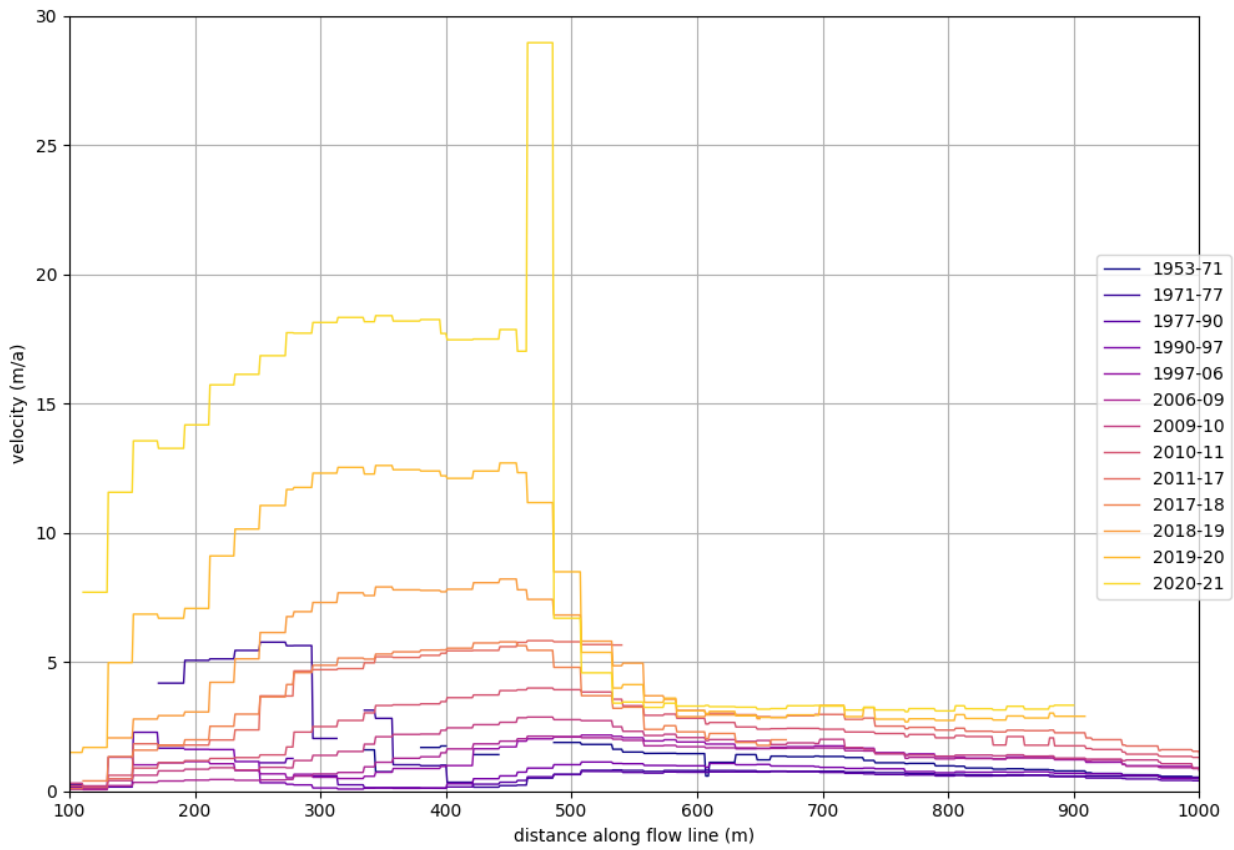


Fig. S5: Velocity (m/a) along the central flow line for all DSM pairs. Data extracted from 20x20m velocity rasters generated from the velocity vectors derived from the DSM pairs.

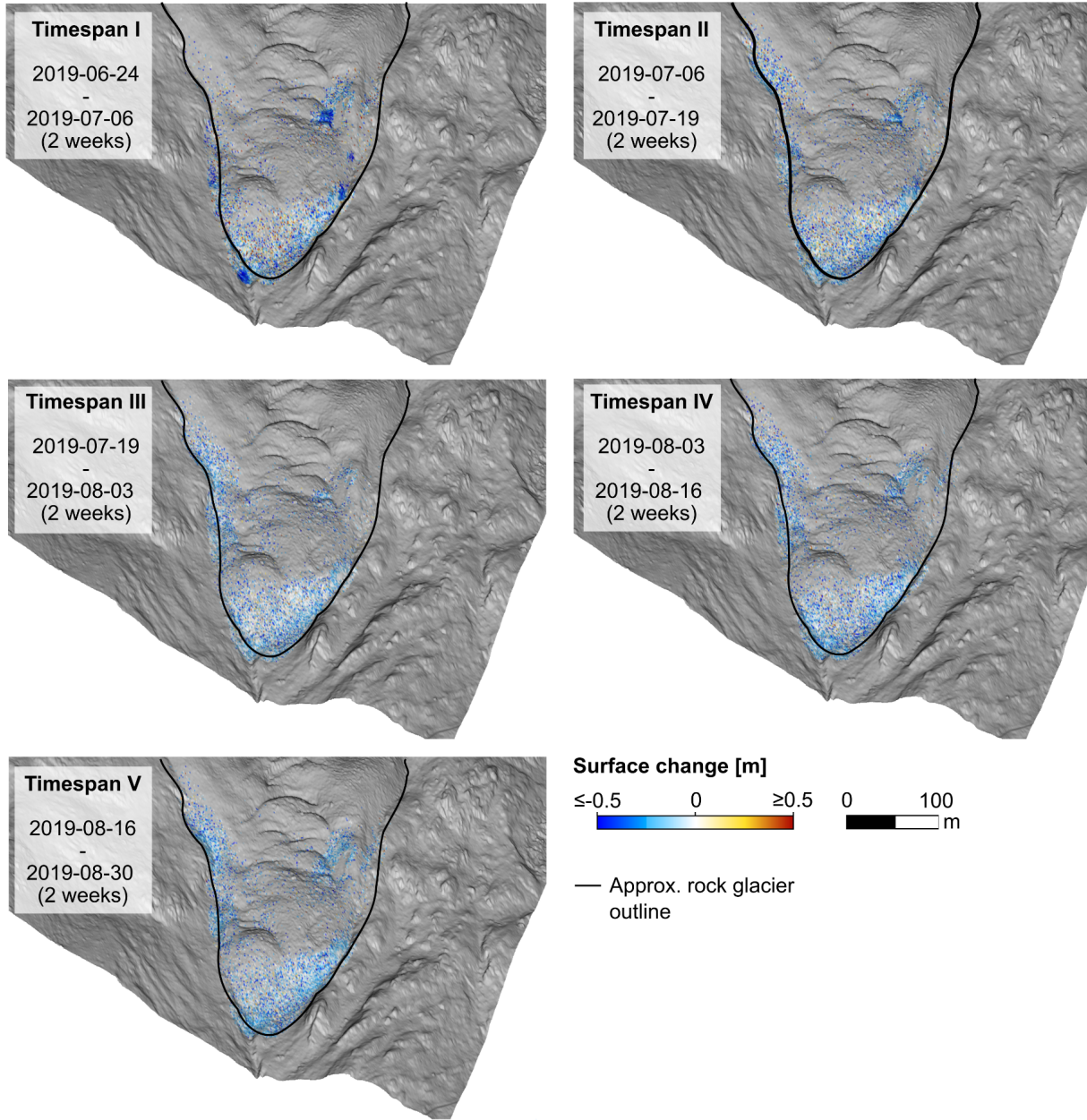


Fig. S6: Magnitudes of surface change in vertical direction derived from the correspondence-driven plane-based M3C2 for 2-week timespans. A hillshade derived from airborne laser scanning data is used as base layer in all subfigures. As the CD-PB M3C2 algorithm favours confident detection of small-magnitude changes over full pointwise change quantification, change information is more dense in at the steep rock glacier front where high point density, spatial coverage and spatial overlap between point clouds of two epochs could be achieved with TLS-based data acquisition.

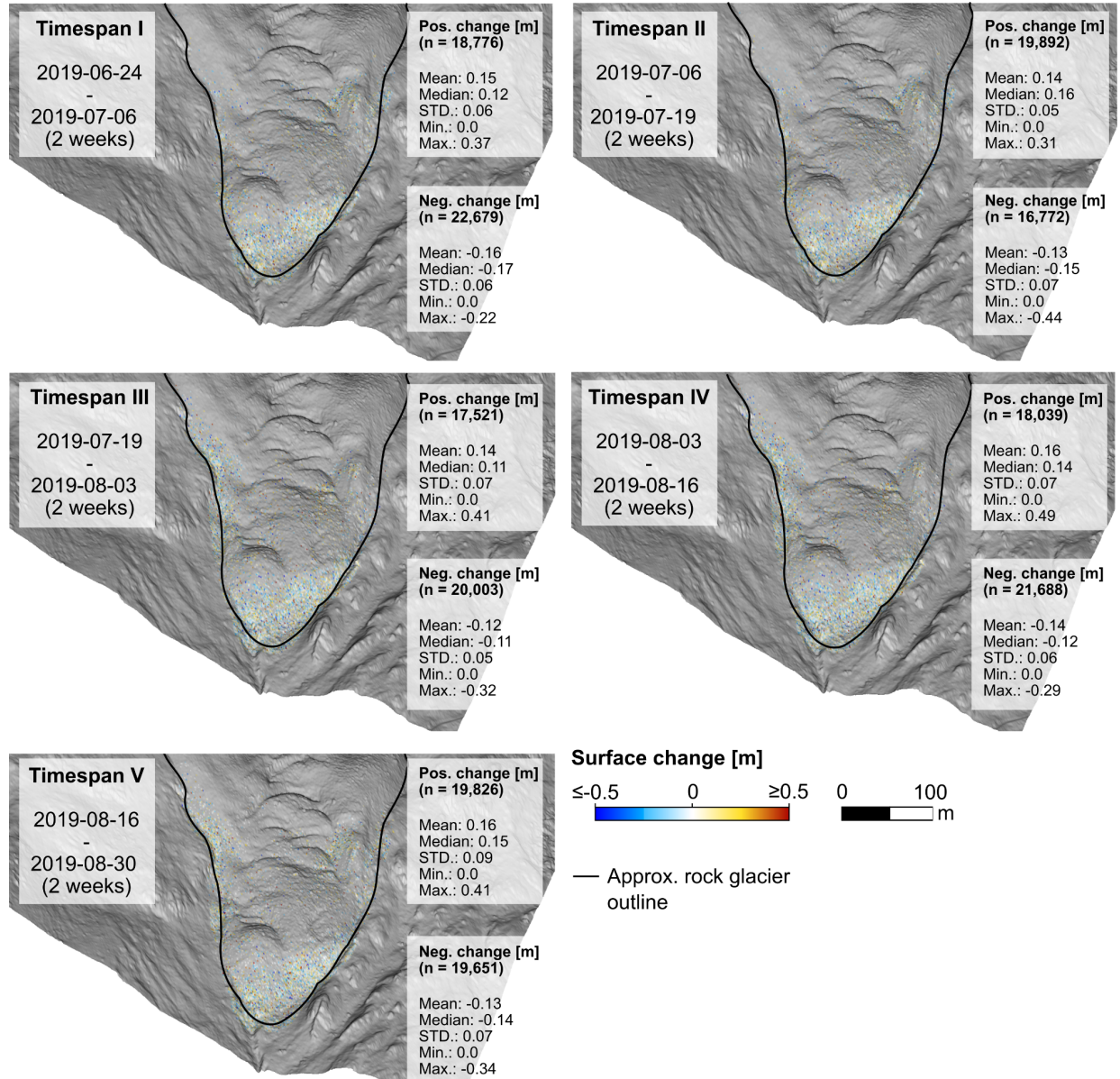


Fig. S7: Magnitudes of surface change in horizontal direction derived from the correspondence-driven plane-based M3C2 for 2-week timespans. A hillshade derived from airborne laser scanning data is used as base layer in all subfigures. As the CD-PB M3C2 algorithm favours confident detection of small-magnitude changes over full pointwise change quantification, change information is more dense in at the steep rock glacier front where high point density, spatial coverage and spatial overlap between point clouds of two epochs could be achieved with TLS-based data acquisition.

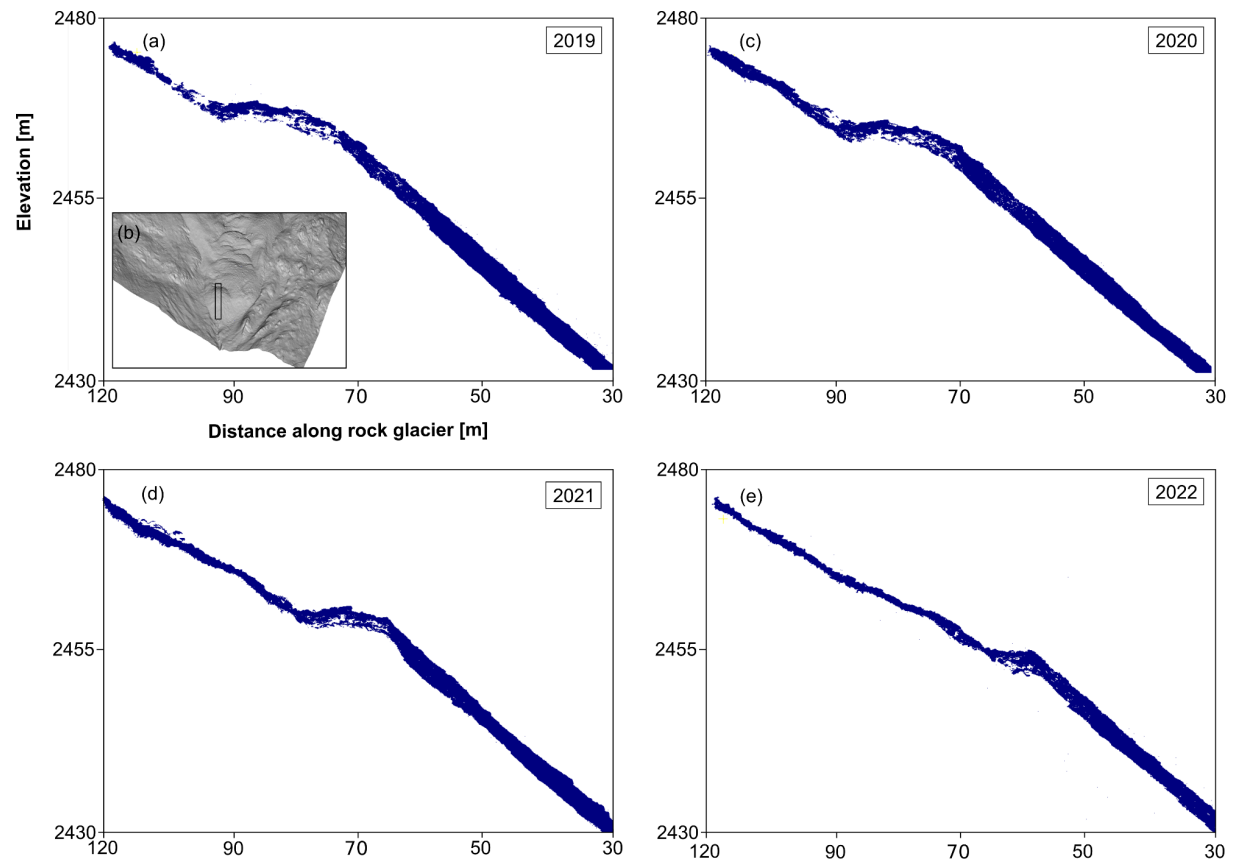


Fig. S8: TLS point clouds for 2019 - 2022 (a, c, d, e) along a convex morphological feature in the lower section of the terminus (b) show the displacement and degradation of the convexity. (Vertical axes show ellipsoidal heights.)

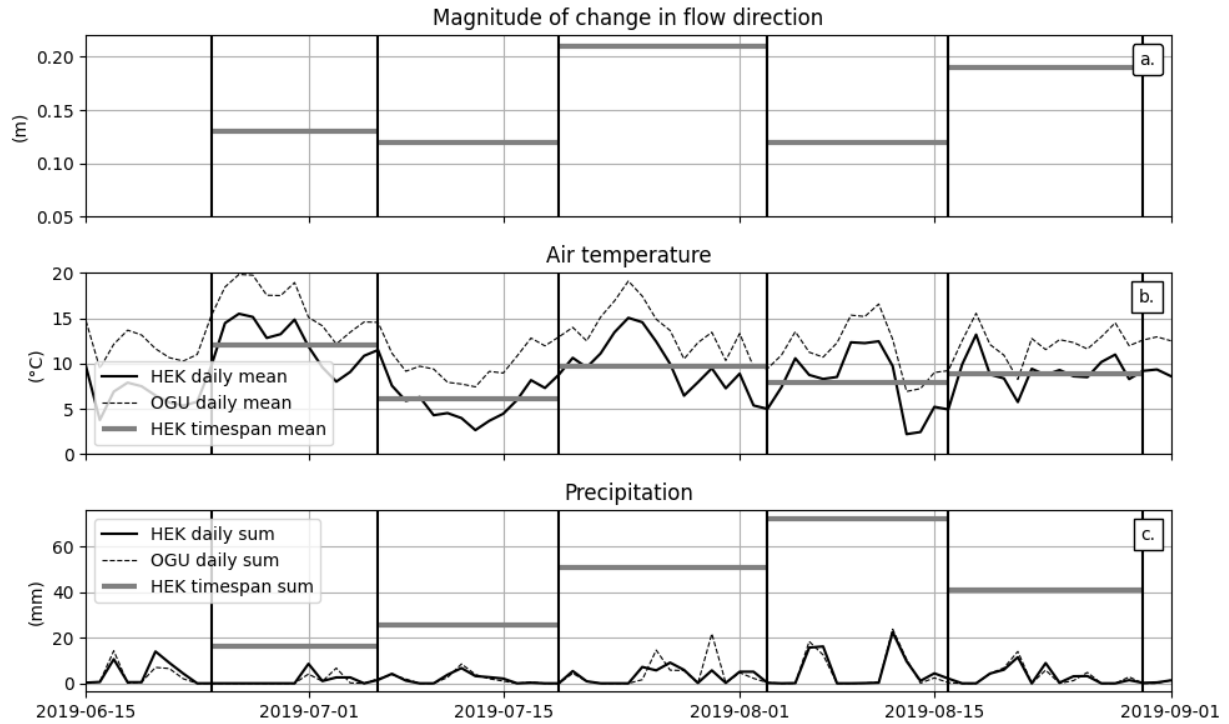


Fig. S9: a) Mean magnitude of change in flow direction at the rock glacier front between TLS epochs during the 2019 summer season. b) Mean daily air temperature at HEK and Obergurgl (OGU) automatic weather stations (AWS), as well as the mean temperature for the duration of each time span between TLS acquisitions. c) Daily precipitation sums at HEK and OGU AWS, as well as precipitation sums for the duration of each timespan. Black vertical lines mark the dates of TLS surveys.

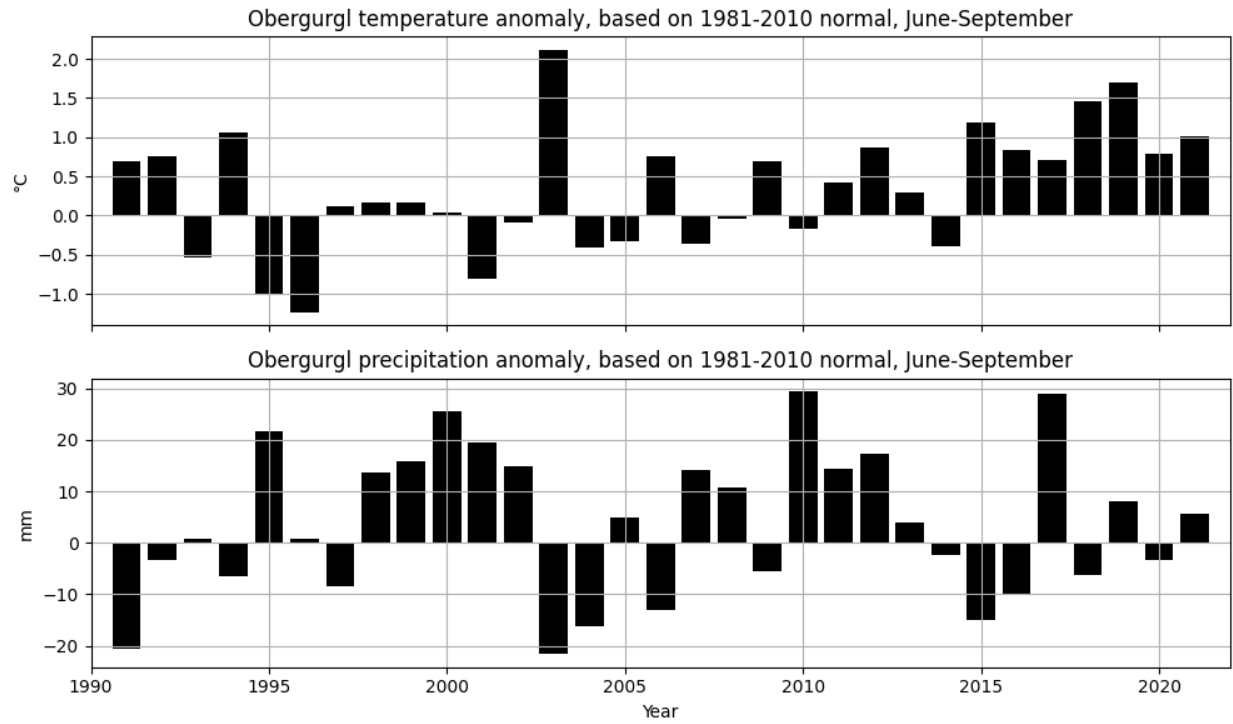


Fig. S10: June-September temperature anomaly (top panel) and precipitation sum anomaly (bottom panel) at the automatic weather station in Obergurgl, both in reference to the 1981-2010 climatological mean. Data: ZAMG data hub (<https://data.hub.zamg.ac.at/>).